Accepted Manuscript

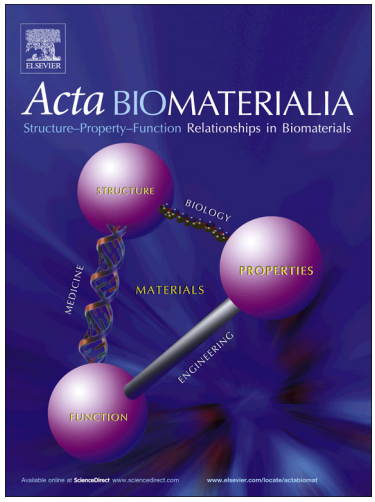

Biocompatible nanostructured solid adhesives for biological soft tissues

Masahiro Okada, Akira Nakai, Emilio Satoshi Hara, Tetsushi Taguchi, Takayoshi Nakano, Takuya Matsumoto

PII: S1742-7061(17)30283-0
DOI: http://dx.doi.org/10.1016/j.actbio.2017.05.014
Reference: ACTBIO 4873

To appear in: *Acta Biomaterialia*

Received Date: 8 February 2017
Revised Date: 16 April 2017
Accepted Date: 3 May 2017

Please cite this article as: Okada, M., Nakai, A., Hara, E.S., Taguchi, T., Nakano, T., Matsumoto, T., Biocompatible nanostructured solid adhesives for biological soft tissues, *Acta Biomaterialia* (2017), doi: http://dx.doi.org/10.1016/j.actbio.2017.05.014

Acta Biomaterialia

Biocompatible nanostructured solid adhesives for biological soft tissues

Masahiro Okada[1], Akira Nakai[1], Emilio Satoshi Hara[1], Tetsushi Taguchi[2], Takayoshi Nakano[3] and Takuya Matsumoto[1,*]

[1] Department of Biomaterials, Graduate School of Medicine, Dentistry and Pharmaceutical Sciences, Okayama University, 2-5-1 Shikata-cho, Kita-ku, Okayama 700-8558, Japan

[2] Polymeric Biomaterials Group, RCFM, National Institute for Materials Science, 1-1 Namiki, Tsukuba, Ibaraki 305-0044, Japan

[3]Division of Materials and Manufacturing Science, Graduate School of Engineering, Osaka University, 2-1 Yamadaoka, Suita, Osaka 565-0871, Japan.

[*]E-mail: tmatsu@md.okayama-u.ac.jp

Abstract

Over the past few years, the development of novel adhesives for biological soft tissue adhesion has gained significant interest. Such adhesives should be non-toxic and biocompatible. In this study, we synthesized a novel solid adhesive using nanostructured hydroxyapatite (HAp) and evaluated its physical adhesion properties through *in vitro* testing with synthetic hydrogels and mice soft tissues. The results revealed that the HAp-nanoparticle dispersions and HAp-nanoparticle-assembled nanoporous plates showed efficient adhesion to the hydrogels. Interestingly, the HAp plates showed different adhesive properties depending upon the shape of their nanoparticles. The HAp plate made up of 17 nm-sized nanoparticles showed an adhesive strength 2.2 times higher than the conventional fibrin glue for mice skin tissues.

Keywords: hydroxyapatite; nanoparticle; solid adhesive; wet adhesion

1. Introduction

Adhesives for soft tissues have been used since 1960 as a substitute for suture [1]. Currently, three main types of tissue adhesives are used clinically: cyanoacrylate[2], gelatin-resorcinol-formaldehyde[3], and fibrin[4]. However, these tissue adhesives suffer either from biocompatibility (for cyanoacrylate and gelatin-resorcinol-formaldehyde adhesives) or bonding strength (for fibrin adhesives) issues [1]. Pressure-sensitive adhesives consisting of synthetic rubbers and tackifiers have also been widely used for skin-contact applications [5]; however, their adhesion effectiveness is relatively low because of their hydrophobic nature.

There has been a significant interest in developing nanostructured solid adhesives, which offer many advantages over conventional pressure-sensitive adhesives [6]. Gecko-inspired nanostructured solid adhesives have been developed with soft organic polymers (polyimide [7] and polyurethane (PU) [8–10]), hard organic polymers (polypropylene[11]), inorganic polymers (polydimethylsiloxane [12–14]), and ceramics (carbon nanotubes [15]). Recently, Rose *et al.* [16] showed that a strong and rapid adhesion between two hydrogels can be achieved by using nanoparticulate adhesives; for example, by spreading a dispersion of SiO_2 nanoparticles in between the two gels. They claimed that the adhesiveness of SiO_2 nanoparticulate adhesives depends on the ability of SiO_2 nanoparticles to adsorb onto polymer gels (and hence SiO_2 nanoparticles act as connectors between the polymer chains) and depends on the ability of polymer chains to reorganize and dissipate energy under stress when adsorbed onto nanoparticles. They also reported that carbon nanotubes and cellulose nanocrystals, which do not

bond hydrogels together, act as adhesives when their surface chemistry is modified. The abovementioned nanostructured solid adhesives are developed for industrial uses. For clinical applications of solid bioadhesives, there is a need for more biocompatible and biodegradable materials.

Hydroxyapatite (HAp) is recognized as a major inorganic component of human hard tissues (bones and teeth), and synthetic HAp, a type of bioceramics, exhibits a high biocompatibility (*i.e.*, nontoxicity) [17,18] and excellent cell adhesion properties [19]. Therefore, HAp and its composites with polymers or metals have been widely used in orthopedic, dental, and tissue engineering applications [20–22]. Other important applications of HAp include their use in drug delivery carriers [23–25] and liquid chromatographic packing [26] by utilizing favorable adsorption capacity of the HAp surface for biomolecules such as proteins [27,28].

In this context, we hypothesized that the adhesiveness of nanoparticulate adhesives for soft tissues would be improved by the use of HAp because of its affinity for extracellular matrix organics [29–31]. Therefore, we first evaluated the application of HAp-nanoparticle dispersions as nanostructured solid adhesives using model hydrogels and then investigated the influence of the morphology of HAp nanoparticles and the solid content of the HAp-nanoparticle dispersions on gel adhesion. Additionally, in order to increase the adhesion strength, HAp-nanoparticle-assembled plates [32,33] were fabricated for application as an adhesive material for hydrogels and mice soft tissues.

2. Materials and methods

2.1. Materials

Unless otherwise mentioned, all materials were of reagent grade and were purchased from Wako Pure Chemical Industries, Ltd. (Osaka, Japan). All materials were used as received. Milli-Q water (Millipore Corp., Bedford, MA, USA) with a specific resistance of 18.2×10^6 Ω·cm was used.

2.2. HAp-nanoparticle dispersions

HAp nanoparticles with different sizes were prepared according to the method described in a previous study [34]. Briefly, an aqueous solution of calcium nitrate (42 mM, 800 mL), whose initial pH was adjusted to 10 by adding a 28% ammonia solution to it, was poured into a 1 L reactor equipped with an inlet for nitrogen and a magnetic stirrer. Once the temperature of the reactor reached a predetermined value (30, 50, or 80 °C), an aqueous solution of diammonium phosphate (100 mM, 200 mL) was added to the reactor at a feed rate of 2 mL/min, and the resultant mixture was stirred for another 24 h at the same temperature. The resulting product was then centrifugally washed until the pH of the solution became neutral. Then, the product was redispersed in water. The concentration of the HAp dispersion was determined by gravimetry. This concentration was adjusted before using the dispersion by adding/removing water to/from it after the centrifugation.

The particle morphology was observed by scanning electron microscopy (SEM) using a JSM-6701F microscope (JEOL Ltd., Tokyo, Japan). The microscope was operated at 5 kV after drying the dispersions. Each dispersion was dried on an aluminum stub and was coated using an osmium coater

(Neoc-Pro, Meiwafosis Co. Ltd., Tokyo, Japan) at an electrical discharge current of 10 mA and a degree of vacuum of 10 Pa for 10 s. The particle size was determined from the SEM images using an image analysis software (Image J; National Institutes of Health (NIH), Bethesda, MD, USA). The particle size was expressed in the form: a number-average value ± standard deviation (N = 50). Product identification (**Fig. S1**) was carried out using X-ray diffraction (XRD) measurements (RINT2500HF; Rigaku Corp., Tokyo, Japan) with Cu Kα radiation (generated at 40 kV and 200 mA) at a scanning rate of 2°/min at room temperature.

2.3. HAp-nanoparticle-assembled plates

Each aqueous dispersion of HAp (4 wt%) was degassed and a part of the degassed dispersions (300 μL) was transferred to a polypropylene (PP) mold (7 mm in width × 7 mm in length × 0.3 mm in thickness), which was prepared by hollowing out the center part of a PP film (0.3 mm in thickness) placed on another PP film. Once the dispersion was dried on the mold at 60 °C for 24 h, a HAp-nanoparticle-assembled plate (5 mm in width × 5 mm in length × 0.1 mm in thickness) was obtained. Note that the HAp plates used for the adhesion tests were in a dry state.

2.4. Synthetic hydrogels

Poly(dimethylacrylamide) (PDMA) gels (water content = 70 wt%) were prepared by solution polymerization and were used as the adherends [35]. The monomer, dimethylacrylamide (DMA), and

the cross-linker, *N,N*'-methylene bisacrylamide (MBA), were used without purification, and the MBA/DMA ratio was set at 0.1 mol%. The redox initiators, potassium persulphate (KPS) and *N,N,N',N'*-tetramethylethylenediamine (TEMED), were used without purification. Just before the polymerization, an aqueous solution (water = 4.05 g) of MBA (5.4 mg), DMA (1.73 g), and TEMED (53 μL) was prepared. Another aqueous solution (water = 4.05 g) of DMA (1.73 g) and KPS (80 mg) was prepared for initiating the redox system. The solution obtained by mixing these two solutions was immediately poured in a silicone mold (120 mm in width × 120 mm in length × 2 mm in thickness) sandwiched between glass plates and polymerized for 20 h at room temperature.

2.5. Mice tissues

All the animal procedures undertaken in this study were strictly in accordance with the Guidelines for Animal Experiments at Okayama University and the experimental protocol was approved by Okayama University (OKU-2015540). Skin, lung, heart, liver, kidney, intestine, and muscle tissues were isolated from 6 week-old female ICR mice (Japan SLC, Inc., Shizuoka, Japan). These tissues were euthanized with CO_2 gas, immersed in a phosphate buffered saline, and used within 1 h after the isolation. The skin tissues were excised from the back of the mice and were trimmed into 40 mm × 5 mm strips.

2.6. Adhesion tests

The PDMA hydrogels prepared according to the procedure described in Section 2.4 were used immediately after being trimmed into strips (5 mm in width × 40 mm in length × 2 mm in thickness), and the surfaces that had attached to glass plates were used for gluing. Two PDMA hydrogels (with an overlapping area of 5 mm × 5 mm) were glued with 10 μL of the HAp aqueous dispersions (concentration = 1, 2, 4, or 6 wt%) or with the HAp-nanoparticle-assembled plate at a contact pressure of 120 kPa for a contact time of 30 s. The trimmed skin tissues (5 mm in width × 40 mm in length; overlapping area = 5 mm × 5 mm) were glued with the HAp plates in the same manner, and the dermic layer side was used for gluing. As a control test, gluing was also done with pure water.

For the control test, a commercially available fibrin glue, Beriplast® P Combi-Set (CSL Behring LLC, PA, USA), was used for gluing the mice skin tissues. Note that the fibrin glue was not used for gluing the PDMA gels. According to the manufacture instruction, solutions with fibrinogen (solution A) and thrombin (solution B) were prepared. A mixture of solution A (25 μL) and solution B (25 μL) was applied on a trimmed skin tissue, and then another skin tissue was placed on the top of this coating (overlapping area = 5 mm × 5 mm) at a pressure of 120 kPa for 30 s.

Just after the gluing, the samples were gripped to screw-type tensile jigs (346-57262-03; Shimadzu Corp., Kyoto, Japan), whose surfaces facing the samples were covered with adhesive-backed #400 silicon carbide sand papers (Buehler, a division of Illinois Tool Works Inc., IL, USA), on a universal testing machine (Ez-test; Shimadzu Corp.) equipped with a load cell of 50 N. The gap in the grip of the tensile jig for the PDMA gels was set at 1.8 mm by gripping the sample with silicone rubber spacers

(thickness = 2 mm), and that for the skin tissue was set at 0.1 mm by gripping the samples without spacers. The adhesion strength tests for the PDMS gels or skin tissues were conducted by pulling the tensile jig, whose initial distance from another jig was set to 5.5 mm, at a speed of 150 mm/min [16] (**Supplemental Movie**). The apparent adhesion strength in this study was calculated from the force-displacement curves (**Fig. S2**) by dividing the maximum load (fracture force) by the overlapping area. Four samples were examined for each test.

The harvested lung, heart, liver, kidney, intestine, and muscle tissues were cut in half and were glued with the HAp plates (5 mm in width × 5 mm in length × 0.1 mm in thickness) at a contact pressure of 120 kPa for a contact time of 30 s.

2.7. Statistical analysis

Once the normality and homogeneity of variance were tested using the Shapiro-Wilk and Bartlett tests, respectively, a one-way variance analysis of the adhesion strengths of the PDMA gels glued with the HAp dispersions (with different concentrations) and HAp plates was carried out. The Tukey-Kramer test was used for comparing these strengths. All statistical tests were performed using R (version 3.3.2) [36] at preset alpha levels of 0.05.

2.8. Water diffusion from PDMA gels into HAp plates

Just after a PDMA gel (5 mm × 5 mm × 2 mm) was attached to a HAp plate (5 mm × 5 mm × 0.1

mm) at the side which was parallel to the plate thickness direction, optical micrographs were sequentially taken near the interface between the PDMA gel and the HAp plate. The HAp plates were relatively transparent in a dry state. However, they turned opaque when water diffused into their pores. The water diffusion distances inside the HAp plates (N=3) were determined after the binarization of the photographs using ImageJ software.

2.9. Histological analysis and Fourier transform infrared spectroscopy

The skin strips were glued with HAp plates, subsequently embedded in a cryosection medium, and immediately frozen thereafter. The cryosections used in this study were obtained according to a previously reported method using adhesive films [37]. These sections (thickness = 10 μm) were then fixed with paraformaldehyde and stained with hematoxylin and eosin (H&E) before being observed under a microscope. For the qualitative analysis (presence of organic materials) of the HAp plates, the attenuated total reflectance Fourier transform infrared (ATR FT-IR) spectra were recorded after pressing the samples on a ZnSe prism equipped on IRAffinity-1S (Shimadzu Corp.) with a resolution of 4 cm^{-1} at 32 scans at room temperature.

3. Results

3.1. Adhesion of synthetic hydrogels with HAp-nanoparticle dispersions

We prepared three kinds of HAp nanoparticles with different particle sizes by wet chemical

synthesis at different temperatures (see **Figs. 1a–c** for SEM images and **Fig. S1** for XRD patterns). The HAp nanoparticles prepared at 30 °C did not show a clear crystal elongation, and the particle size was 17 ± 3 nm (**Fig. 1a**), whereas those obtained at higher temperatures showed rod-shaped morphologies and the particle size increased with an increase in the reaction temperature (154 ± 13 nm along the longer axis and 13 ± 4 nm along the shorter axis for the particles prepared at 50 °C; 585 ± 44 nm along the longer axis and 43 ± 15 nm along the shorter axis for the particles prepared at 80 °C) (**Figs. 1a** and **1b)**. The HAp nanoparticles prepared in this study at 30, 50, and 80 °C will henceforth be referred to as S-Hap, M-Hap, and L-HAp, respectively.

The typical force-displacement curves and the apparent adhesion strengths between two PDMA hydrogels glued with the aqueous dispersions of HAp nanoparticles (of different morphologies) with different concentrations (solid content) are shown in **Figs. 1d** and **1e**, respectively. All the samples rotated to around 35° just before the separation (**Fig. S3**), indicating that the glued regions experienced both shear and tensile stresses during the adhesion tests. The apparent adhesion strength of the PDMA hydrogels glued with the HAp dispersions with a concentration of less than 1 wt% showed no significant difference compared to that of the hydrogels glued with pure water (control group). The SEM analysis results revealed that in the case of the S-HAp and M-HAp dispersions, the fractured surface hardly contained any nanoparticles (**Figs. S4a and S4b**). In the case of the L-HAp dispersion (**Figs. S4c**), a part of the HAp nanoparticles remained on the PDMA overlapped area after the adhesion tests. By increasing the concentration of each HAp dispersion, the surface coverage of the PDMA overlapped area (by HAp

nanoparticles) increased, and at a higher concentration (6 wt%), most of the PDMA glued areas were covered with HAp nanoparticles (**Fig. S5**), indicating that the cohesive fracture among the HAp nanoparticles was dominant in all the cases.

3.2. Adhesion of synthetic hydrogels with HAp-nanoparticle-assembled plates

In order to improve the cohesive strength among the HAp nanoparticles, the nanoparticle dispersions were dried at 60 °C [32,33], and HAp-nanoparticle-assembled plates (*i.e.*, dried porous monoliths consisting of interconnected HAp nanoparticles) were prepared (**Figs. 2a–c**). The HAp plates showed an improved adhesion strength compared to the HAp dispersions (**Fig. S6**). A comparison of the initial HAp nanoparticle sizes of the plates revealed that the apparent adhesion strengths of the S-HAp and M-HAp plates were greater than that of the L-HAp plates (**Fig. 2d**). Note that the PDMA gels broke near the overlapped area after all the adhesion tests with the S-HAp plates (**Fig. S7**), indicating the cohesive fracture of the PDMA adherends. On the other hand, the PDMA gels inside the overlapped area were broken in some cases (50%) and in all the cases (100%) when the M-HAp and L-HAp plates were used, respectively. The SEM images of the fractured surfaces showed some dents on the gels. These dents are attributed to the cohesive fracture of PDMA. The M-HAp and L-HAp plate surfaces (**Fig. S8**) showed protrusions, corresponding to the dents on the gel surfaces. These results indicate the cohesive fracture of both the PDMA adherend and HAp plate in the case of the M-HAp and L-HAp plates. After the contact of a hydrogel and an S-HAp plate, the water in the hydrogel diffused into the HAp plate (**Fig.**

3).

3.3. Adhesion of mice soft tissues with HAp-nanoparticle-assembled plates

To evaluate the potential use of HAp-nanoparticle-assembled plates as soft tissue adhesives, mice soft tissues (*e.g.*, lungs, kidney, and muscles) were isolated, cut in half, and glued with the HAp plates. As shown in **Fig. 4a**, the S-HAp plates could glue a variety of mice soft tissues. In the case of the skin tissues glued with the S-HAp plates (**Figs. 4b–d**), the adhesion strength was 44 ± 13 kPa, which was significantly higher than that obtained with a commercially available fibrin glue, Beriplast® (18 ± 9 kPa). The adhesion strengths of the other tissues could not be determined because of the breakage of the tissue during trimming or after gripping to the jigs.

In order to investigate the mechanism behind the adhesion of the HAp plates with the skin tissues, their histological sections were prepared. **Figure 5** shows the histological sections of the skin tissues before and after gluing with the S-HAp plate and the SEM images of the overlapped skin tissue surfaces after the adhesion tests. The histological sections were stained with H&E (dark blue for hematoxylin and light pink for eosin). Once the skin tissues were glued with the HAp plate, the light pink regions corresponding to the tissue matrix condensed near the surface of the HAp plate. The SEM images also showed the condensed tissue matrix created on the surface of the skin tissues after the adhesion tests. Moreover, some remnant fibers were observed on the HAp surface after the adhesion tests (**Fig. 5b-vi**). The ATR FT-IR results also suggested that some proteins and lipids remained on the HAp surface after

the adhesion tests (**Fig. 6**). These results indicate that a high affinity existed between the tissue matrix and the HAp plates.

4. Discussion

First, we conducted adhesion tests using a synthetic PDMA hydrogel (water content, 70 wt%) cross-linked with MBA as a model adherend based on the method described by Rose *et al.*[16] using SiO_2 nanoparticle dispersions. The aqueous dispersions of HAp nanoparticles (of different sizes) with different concentrations were used as the adhesives. Note that for the same PDMA width (5 mm) and thickness (2 mm), the fracture force at the overlap length (5 mm) for the 6 wt% dispersion of 17 nm-sized HAp nanoparticles (fracture force = ~120 mN) was larger than that for the 52 wt% dispersion of 15 nm-sized SiO_2 nanoparticles (fracture force = ~90 mN [16]). The adhesion strength was determined not only by the interaction between the adhesive particles and the adherends (*i.e.*, interfacial failure) but also by the interaction among the adhesive particles (*i.e.*, cohesive failure of the adhesive). This is because the nanoparticle adhesives were not monolayered, but multilayered and consisted of accumulated nanoparticles, as discussed below. Although the concentration of the dispersion (6 wt%) in our case was quite different from that in Rose's work (52 wt%), the lower fracture load obtained by Rose *et al.* for their dispersion (0.3 $\mu L/mm^2$) of 15 nm-sized SiO_2 nanoparticles can be attributed to the thicker adhesive layers in their case.

Judging from the thickness (less than 43 nm) of the HAp nanoparticles and the amount (10 μL) of

the dispersion under assumption of the density of HAp is 3.16 g/cm^3 [38], an HAp concentration of approximately 0.03 wt% is sufficient to completely cover the overlapped region of the PDMA hydrogels (5 mm × 5 mm) by a monolayer of the nanoparticles. However, the adhesion strength of the PDMA hydrogels glued with the HAp dispersions with a concentration of less than 1 wt% showed no significant difference compared to the samples glued with pure water (control group). This can be explained in part by the fact that almost all the nanoparticles were pressed out from the PDMA overlapped area because of the outflow of water during the gluing (pressing at 120 kPa for 30 s) except for the L-HAp nanoparticles. In the case of the 1 wt% L-HAp dispersion, a part of the HAp nanoparticles remained on the PDMA overlapped area possibly because of their large size and morphology; *i.e.*, because of the smaller diffusion coefficient of the larger rod-shaped nanoparticles [39]. Eventually the remaining L-HAp nanoparticles could promote a stronger adhesion compared to the S-HAp and M-HAp nanoparticle dispersions at low concentrations of 2 and 4 wt%.

It has been shown that DMA oligomers interact with the HAp surface [40]. This interaction is believed to occur through the phosphate groups (P sites) present on the *c*-plane of the HAp surface [26]. S-HAp, which did not show a clear crystal elongation, was expected to have a predominant *c*-plane surface as compared to the rod-shaped HAp nanoparticles, which had large *a*-planes because of the elongation of the *c*-axis of the HAp lattice [41]. However, the degree of interfacial fracture, which was estimated from the surface uncoverage ratio of PDMA by the HAp nanoparticles (28% for S-HAp, 16% for M-HAp, and 3% for L-HAp), was the largest in the case of the S-HAp dispersion. These results

suggest that the cohesive strength among the S-HAp nanoparticles was larger than the interfacial adhesion strength between HAp and PDMA. This may be because of the larger particle coordination number of the S-HAp nanoparticles as compared to that of the rod-shaped nanoparticles. At 6 wt%, which is the maximum concentration above which the dispersions could not be applied with a pipette because of their large viscosities, the adhesion strength increased; however, the cohesive fracture of the HAp nanoparticle aggregates was dominant.

Therefore, HAp-nanoparticle-assembled plates (*i.e.*, dried porous monoliths consisting of interconnected HAp nanoparticles) were fabricated by drying the nanoparticle dispersions, in order to improve the interaction among the HAp nanoparticles. The HAp plate showed an improved adhesion strength for the PDMA hydrogels compared to the HAp dispersions. A comparison of the influence of the nanoparticle size of the HAp plates on their adhesion strengths revealed that the adhesion strength of S-HAp plate consisting of the smaller nanoparticles was larger than that of the M-HAp and L-HAp plates, which can also be associated with the presence of phosphate groups (P sites) on the *c*-plane of the S-HAp surface, as discussed above. HAp has a relatively large polar fraction (γ_{sv}^{p}, 65.8%) of surface tension (γ_{sv}, 46.7 mJ/m^2) [42]. Hence, the capillary binding of water (the formation of a liquid water meniscus bridge) between the HAp plates and the hydrogels was also expected to increase the adhesion force. Besides, HAp plates have nanosized roughness because of their nanoparticle morphology and also have nanosized pores between the nanoparticles (typical pore size of 8 nm for smaller-nanoparticle-assembled plates of 110 nm for rod-shaped-nanoparticle-assembled plates [32]).

The capillary force between hydrophilic solid surfaces increases by decreasing their nanosized roughness [43] and pore size [44]. Hence, another reason why the S-HAp plate showed the highest adhesion strength should be the enhanced capillary binding between it and the gel.

The S-HAp plate could also be used as potential soft tissue adhesives. The adhesion strength between the skin tissues (adherend) and the S-HAp plate (adhesive) was markedly higher than that between the skin tissues and the commercially available fibrin glues (2.2 ± 1.3 kPa [45] for Tissucol® and 18 ± 9 kPa for Beriplast®). Besides, the adhesion strength for the skin tissues (44 ± 13 kPa) was higher than that for the PDMA hydrogels (8.0 ± 0.5 kPa) possibly because of the large cohesive strength of the adherends (*i.e.*, the larger tensile strength of the skin tissues). Another reason for the improved adhesion strength for the skin tissues could be the formation of a condensed matrix layer, which seemed to be formed because of the ultrafiltration effect of the nanoporous HAp plate. Water diffused from the tissues into the plate, which had hydrophilic open pores (porosity = ~50 vol% [32]). Prior to the attachment of the plate to the tissues or hydrogels, these pores were dry and were not filled with water. After the attachment, water molecules diffused into these pores, whereas the larger extracellular matrix (ECM) molecules (such as collagen fibers) could not diffuse into them because of their small size (pore size = 8 nm [32]). These ECM molecules then condensed on the HAp plate. Such a condensation is likely to increase the interaction points between the HAp surface and the ECM molecules. By taking into account the water diffusion rate and thickness (10–20 μm) of the condensed layer of the skin tissues observed in the histological section stained with H&E, it can be concluded that the condensed tissue

layer formed immediately after the contact of the skin tissues with the HAp plate. In summary, the improved adhesion strength of the nanoporous HAp plate for soft tissues can be attributed to (1) the ability of HAp to adsorb onto ECM molecules [29–31], (2) the condensation of ECM molecules by the ultrafiltration effect of the nanoporous HAp plate, and (3) the water capillary binding between the HAp plate and the adherend. Note that cyanoacrylates- or glutaraldehyde-based soft tissue adhesives have an adhesive strength an order of magnitude higher (~170 kPa [46]) than that of fibrin glues. On the basis of the SEM observations and ATR FT-IR measurements for the fractured surface of the HAp plates (after the adhesion with the skin tissues), it can be stated that the interfacial fracture between the skin tissues and the HAp plates was dominant. Therefore, in order to improve the adhesion strength further, the surface modification of HAp nanoparticles with ion substitutions [47,48] and/or amino acids [25,49] should be an effective method because these modifications enhance the protein adsorption capacity and stability on HAp surfaces. Moreover, controlling the surface-induced self-assembly of ECM molecules, which affects the adsorbed structures and properties of ECM molecules (*i.e.*, their rigidity and packing behaviors [50]), is also important.

It is noteworthy that, in this study, HAp-sintered ceramics, which can be commonly obtained by sintering at around 1,000 °C, were not used because HAp ceramics are hardly degradable in a living body, whereas HAp nanoparticles are degradable because of their enhanced solubility [51] and endocytosis [52,53]. The HAp-nanoparticle-assembled plates prepared by drying the HAp nanoparticle dispersions at 60 °C could not disperse completely in aqueous media even after a thorough ultrasound

irradiation [33], suggesting the generation of strong interactions between the nanoparticles after drying. Although a high internal cohesiveness is important to enhance the adhesion strength, the biodegradability of HAp-nanoparticle-assembled plates might decrease compared with HAp-nanoparticle dispersions. The biodegradability of HAp plates should be optimized to match the healing of the tissues of interest by controlling the initial size of HAp nanoparticles (by optimizing wet chemical precipitation conditions) and the interconnectivity between them (by optimizing dry and surface modification conditions). The use of composite materials is also believed to be an effective way to control the biodegradability as well as the mechanical properties of HAp nanoparticle based adhesives, as discussed below.

Fibroblasts are known to sense and respond to the mechanical properties of substrates [54], and the stiffness turning of adhesives to match the soft tissues should be important to aid the repair of injured tissues [55]. Since the HAp-nanoparticle-assembled plates prepared here had a brittle nature and a much higher stiffness than soft tissues, it is important to develop HAp composites with flexible polymers. For developing such composites, a simple mixing of HAp nanoparticles with polymers will be not effective because the nanopores among the HAp nanoparticles should be buried and the hydrophilic surface of HAp should be covered with the polymer matrix. Creating a nanoparticle coating on nanoporous biodegradable polymers would be an effective way to fabricate solid-state tissue adhesives with enhanced adhesion strength and optimized mechanical and biodegradable properties. In this paper, we reported the physical adhesion property of HAp dispersions or HAp plates to hydrogels including

isolated soft tissues. The biological properties of HAp composite adhesives including their wound healing ability and biodegradability will be reported in the near future.

4. Conclusion

The adhesion properties of biocompatible HAp-nanoparticle dispersions and nanoparticle-assembled plates were investigated. The HAp-nanoparticle dispersions and nanoparticle-assembled plates showed a convenient adhesion to synthetic hydrogels. Moreover, the HAp plates showed an enhanced adhesion to biological soft tissues. Although the HAp nanoparticle-based adhesives reported here need to be improved in terms of the adhesion strength, mechanical properties, and biodegradability for clinical applications, our results will help in developing an efficient approach to close incised soft tissues with better adhesion strength as well as biocompatibility and finding novel ways to integrate soft tissues with synthetic hydrogels (such as drug reservoirs) by using nanostructured bioceramic adhesives.

Acknowledgements

This work was supported partly by the Japan Society for the Promotion of Science KAKENHI (grant numbers: JP15K1572307, JP25220912, and JP25293402) and partly by the Matching Planner Program (MP27115663113) from Japan Science and Technology Agency.

References

[1] M. Matsuda, M. Inoue, T. Taguchi, Adhesive properties and biocompatibility of tissue adhesives composed of various hydrophobically modified gelatins and disuccinimidyl tartrate, J. Bioact. Compat. Polym. 27 (2012) 481–498. doi:10.1177/0883911512455116.

[2] Y.-C. Tseng, H. Suong-Hyu, Y. Ikada, Y. Shimizu, K. Tamura, S. Hitomi, In vivo evaluation of 2-cyanoacrylates as surgical adhesives, J. Appl. Biomater. 1 (1990) 111–119.

[3] S. Fukunaga, M. Karck, W. Harringer, J. Cremer, C. Rhein, A. Haverich, The use of gelatin-resorcin-formalin glue in acute aortic dissection type A, Eur. J. Cardio-Thoracic Surg. 15 (1999) 564–570. doi:10.1016/S1010-7940(99)00084-6.

[4] E. V Dare, M. Griffith, P. Poitras, T. Wang, G.F. Dervin, A. Giulivi, M.T. Hincke, Fibrin sealants from fresh or fresh/frozen plasma as scaffolds for in vitro articular cartilage regeneration., Tissue Eng. Part A. 15 (2009) 2285–97. doi:10.1089/ten.tea.2008.0228.

[5] S. Venkatraman, R. Gale, Skin adhesives and skin adhesion. 1. Transdermal drug delivery systems., Biomaterials. 19 (1998) 1119–36. http://www.ncbi.nlm.nih.gov/pubmed/9720896 (accessed May 4, 2016).

[6] K. Jin, Y. Tian, J.S. Erickson, J. Puthoff, K. Autumn, N.S. Pesika, Design and fabrication of Gecko-inspired adhesives, Langmuir. 28 (2012) 5737–5742. doi:10.1021/la204040p.

[7] A.K. Geim, S. V Dubonos, I. V Grigorieva, K.S. Novoselov, a a Zhukov, S.Y. Shapoval, Microfabricated adhesive mimicking gecko foot-hair., Nat. Mater. 2 (2003) 461–463. doi:10.1038/nmat917.

[8] M.P. Murphy, B. Aksak, M. Sitti, Gecko-Inspired Directional and Controllable Adhesion, Small. 5 (2008) 170–175. doi:10.1002/smll.200801161.

[9] B. Aksak, M.P. Murphy, M. Sitti, Adhesion of Biologically Inspired Vertical and Angled Polymer Microfiber Arrays, Langmuir. 23 (2007) 3322–3332. doi:10.1021/la062697t.

[10] H.E. Jeong, J.-K. Lee, H.N. Kim, S.H. Moon, K.Y. Suh, A nontransferring dry adhesive with hierarchical polymer nanohairs, Proc. Natl. Acad. Sci. 106 (2009) 5639–5644. doi:10.1073/pnas.0900323106.

[11] J. Lee, R.S. Fearing, K. Komvopoulos, Directional adhesion of gecko-inspired angled microfiber arrays, Appl. Phys. Lett. 93 (2008) 2006–2009. doi:10.1063/1.3006334.

[12] C. Greiner, E. Arzt, A. del Campo, Hierarchical Gecko-Like Adhesives, Adv. Mater. 21 (2009) 479–482. doi:10.1002/adma.200801548.

[13] D. Sameoto, C. Menon, Direct molding of dry adhesives with anisotropic peel strength using an offset lift-off photoresist mold, J. Micromechanics Microengineering. 19 (2009) 115026. doi:10.1088/0960-1317/19/11/115026.

[14] J. Yu, S. Chary, S. Das, J. Tamelier, N.S. Pesika, K.L. Turner, J.N. Israelachvili, Gecko-Inspired Dry Adhesive for Robotic Applications, Adv. Funct. Mater. 21 (2011) 3010–3018. doi:10.1002/adfm.201100493.

[15] B. Yurdumakan, N.R. Raravikar, P.M. Ajayan, A. Dhinojwala, Synthetic gecko foot-hairs from multiwalled carbon nanotubes., Chem. Commun. (Camb). 405 (2005) 3799–3801. doi:10.1039/b506047h.

[16] S. Rose, A. Prevoteau, P. Elzière, D. Hourdet, A. Marcellan, L. Leibler, Nanoparticle solutions as adhesives for gels and biological tissues., Nature. 505 (2014) 382–5. doi:10.1038/nature12806.

[17] E.I. Abdel-Gawad, S.A. Awwad, Biocompatibility of Intravenous Nano Hydroxyapatite in Male Rats, Nat. Sci. 8 (2010). http://www.sciencepub.net/nature (accessed May 9, 2016).

[18] D.M. Lawton, M.D.J. Lamaletie, D.L. Gardner, Biocompatibility of hydroxyapatite ceramic: response of chondrocytes in a test system using low temperature scanning electron microscopy, J. Dent. 17 (1989) 21–27. doi:10.1016/0300-5712(89)90003-1.

[19] S. V Dorozhkin, Nanosized and nanocrystalline calcium orthophosphates., Acta Biomater. 6 (2010) 715–34. doi:10.1016/j.actbio.2009.10.031.

[20] M. Honda, T.J. Fujimi, S. Izumi, K. Izawa, M. Aizawa, H. Morisue, T. Tsuchiya, N. Kanzawa, Topographical analyses of proliferation and differentiation of osteoblasts in micro- and macropores of apatite-fiber scaffold., J. Biomed. Mater. Res. A. 94 (2010) 937–44. doi:10.1002/jbm.a.32779.

[21] S.-W. Choi, Y. Zhang, S. Thomopoulos, Y. Xia, In vitro mineralization by preosteoblasts in poly(DL-lactide-co-glycolide) inverse opal scaffolds reinforced with hydroxyapatite nanoparticles., Langmuir. 26 (2010) 12126–31. doi:10.1021/la101519b.

[22] M. Okada, T. Matsumoto, Synthesis and modification of apatite nanoparticles for use in dental

and medical applications, Jpn. Dent. Sci. Rev. 51 (2015) 85–95. doi:10.1016/j.jdsr.2015.03.004.
[23] K. Tomoda, H. Ariizumi, T. Nakaji, K. Makino, Hydroxyapatite particles as drug carriers for proteins, Colloids Surfaces B Biointerfaces. 76 (2010) 226–235. doi:10.1016/j.colsurfb.2009.10.039.
[24] A. Bouladjine, A. Al-Kattan, P. Dufour, C. Drouet, New advances in nanocrystalline apatite colloids intended for cellular drug delivery., Langmuir. 25 (2009) 12256–65. doi:10.1021/la901671j.
[25] T. Matsumoto, M. Okazaki, M. Inoue, S. Yamaguchi, T. Kusunose, T. Toyonaga, Y. Hamada, J. Takahashi, Hydroxyapatite particles as a controlled release carrier of protein, Biomaterials. 25 (2004) 3807–3812. doi:10.1016/j.biomaterials.2003.10.081.
[26] T. Kawasaki, Hydroxyapatite as a liquid chromatographic packing, J. Chromatogr. 544 (1991) 147–184.
[27] K.L. Kilpadi, P.L. Chang, S.L. Bellis, Hydroxylapatite binds more serum proteins, purified integrins, and osteoblast precursor cells than titanium or steel., J. Biomed. Mater. Res. 57 (2001) 258–67. http://www.ncbi.nlm.nih.gov/pubmed/11484189 (accessed May 9, 2016).
[28] J.S. Lee, A.J. Wagoner Johnson, W.L. Murphy, A modular, hydroxyapatite-binding version of vascular endothelial growth factor, Adv. Mater. 22 (2010) 5494–5498. doi:10.1002/adma.201002970.
[29] M. Tagaya, T. Ikoma, T. Takemura, N. Hanagata, T. Yoshioka, J. Tanaka, Effect of interfacial proteins on osteoblast-like cell adhesion to hydroxyapatite nanocrystals., Langmuir. 27 (2011) 7645–53. doi:10.1021/la200621p.
[30] H. Fujita, T. Kudo, H. Kanetaka, T. Miyazaki, M. Hashimoto, M. Kawashita, Adsorption of Laminin on Hydroxyapatite and Alumina and the MC3T3-E1 Cell Response, ACS Biomater. Sci. Eng. 2 (2016) 1162–1168. doi:10.1021/acsbiomaterials.6b00190.
[31] F. Wu, D.D.W. Lin, J.H. Chang, C. Fischbach, L.A. Estroff, D. Gourdon, Effect of the materials properties of hydroxyapatite nanoparticles on fibronectin deposition and conformation, Cryst. Growth Des. 15 (2015) 2452–2460. doi:10.1021/acs.cgd.5b00231.
[32] M. Uehira, M. Okada, S. Takeda, N. Matsumoto, Preparation and characterization of low-crystallized hydroxyapatite nanoporous plates and granules, Appl. Surf. Sci. 287 (2013) 195–202. doi:10.1016/j.apsusc.2013.09.117.
[33] M. Okada, T. Furuzono, Low-temperature synthesis of nanoparticle-assembled, transparent, and low-crystallized hydroxyapatite blocks, J. Colloid Interface Sci. 360 (2011) 457–462. doi:10.1016/j.jcis.2011.04.068.
[34] M. Okada, D. Hiramatsu, T. Okihara, T. Matsumoto, Adsorption and desorption behaviors of cetylpyridinium chloride on hydroxyapatite nanoparticles with different morphologies, Dent. Mater. J. 35 (2016) 651–658. doi:10.4012/dmj.2015-420.
[35] L. Carlsson, S. Rose, D. Hourdet, A. Marcellan, Nano-hybrid self-crosslinked PDMA/silica hydrogels, Soft Matter. 6 (2010) 3619. doi:10.1039/c0sm00009d.
[36] R.C. Team, R: A Language and Environment for Statistical Computing, (2016).
[37] T. Kawamoto, M. Shimizu, A method for preparing 2- to 50-micron-thick fresh-frozen sections of large samples and undecalcified hard tissues., Histochem. Cell Biol. 113 (2000) 331–9. http://www.ncbi.nlm.nih.gov/pubmed/10883392 (accessed September 7, 2016).
[38] M. Descamps, L. Boilet, G. Moreau, A. Tricoteaux, J. Lu, A. Leriche, V. Lardot, F. Cambier, Processing and properties of biphasic calcium phosphates bioceramics obtained by pressureless sintering and hot isostatic pressing, J. Eur. Ceram. Soc. 33 (2013) 1263–1270. doi:10.1016/j.jeurceramsoc.2012.12.020.
[39] J. Sun, F. Wang, Y. Sui, Z. She, W. Zhai, C. Wang, Y. Deng, Effect of particle size on solubility, dissolution rate, and oral bioavailability: evaluation using coenzyme Q□□ as naked nanocrystals., Int. J. Nanomedicine. 7 (2012) 5733–44. doi:10.2147/IJN.S34365.
[40] H. Takashima, K. Iwaki, R. Furukuwa, K. Takishita, H. Sawada, Preparation and applications of a variety of fluoroalkyl end-capped oligomer/hydroxyapatite composites, J. Colloid Interface Sci. 320 (2008) 436–444. doi:10.1016/j.jcis.2007.12.029.
[41] M. Okada, K. Furukawa, T. Serizawa, Y. Yanagisawa, H. Tanaka, T. Kawai, T. Furuzono, Interfacial Interactions between Calcined Hydroxyapatite Nanocrystals and Substrates, Langmuir. 25 (2009) 6300–6306. doi:10.1021/la804274q.
[42] M.A. Lopes, F.J. Monteiro, J.D. Santos, A.P. Serro, B. Saramago, Hydrophobicity , surface tension , and zeta potential measurements of glass-reinforced hydroxyapatite composites, J Biomed Mater Res. 45 (1999) 370–5.

[43] P.J. van Zwol, G. Palasantzas, J.M. Th De Hosson, Influence of roughness on capillary forces between hydrophilic surfaces, Pysical Rev. E. 78 (2008) 31606. doi:10.1103/PhysRevE.78.031606.
[44] M. Fuji, K. Machida, T. Takei, T. Watanabe, M. Chikazawa, Effect of Surface Geometric Structure on the Adhesion Force between Silica Particles, J. Phys. Chem. B. 102 (1998) 8782–8787. doi:10.1021/jp981978+.
[45] S. Kull, I. Martinelli, E. Briganti, P. Losi, D. Spiller, S. Tonlorenzi, G. Soldani, Glubran2 Surgical Glue: In Vitro Evaluation of Adhesive and Mechanical Properties, J. Surg. Res. 157 (2009) e15–e21. doi:10.1016/j.jss.2009.01.034.
[46] N. V Shah, R. Meislin, Current state and use of biological adhesives in orthopedic surgery., Orthopedics. 36 (2013) 945–56. http://www.ncbi.nlm.nih.gov/pubmed/24579215 (accessed March 29, 2017).
[47] E. Fujii, M. Ohkubo, K. Tsuru, S. Hayakawa, A. Osaka, K. Kawabata, C. Bonhomme, F. Babonneau, Selective protein adsorption property and characterization of nano-crystalline zinc-containing hydroxyapatite, Acta Biomater. 2 (2006) 69–74. doi:10.1016/j.actbio.2005.09.002.
[48] K. Kandori, S. Toshima, M. Wakamura, M. Fukusumi, Y. Morisada, Effects of Modification of Calcium Hydroxyapatites by Trivalent Metal Ions on the Protein Adsorption Behavior, J. Phys. Chem. B. 114 (2010) 2399–2404. doi:10.1021/jp911783r.
[49] T. Matsumoto, M. Okazaki, M. Inoue, Y. Hamada, M. Taira, J. Takahashi, Crystallinity and solubility characteristics of hydroxyapatite adsorbed amino acid, Biomaterials. 23 (2002) 2241–2247. doi:10.1016/S0142-9612(01)00358-1.
[50] J.-H. Lin, H.-Y. Chang, W.-L. Kao, K.-Y. Lin, H.-Y. Liao, Y.-W. You, Y.-T. Kuo, D.-Y. Kuo, K.-J. Chu, Y.-H. Chu, J.-J. Shyue, Effect of Surface Potential on Extracellular Matrix Protein Adsorption, Langmuir. 30 (2014) 10328–10335. doi:10.1021/la5020362.
[51] D. Smoleń, T. Chudoba, S. Gierlotka, A. Kedzierska, W. Łojkowski, K. Sobczak, W. Święszkowski, K.J. Kurzydłowski, Hydroxyapatite nanopowder synthesis with a programmed resorption rate, J. Nanomater. 2012 (2012). doi:10.1155/2012/841971.
[52] I.W. Bauer, S.-P. Li, Y.-C. Han, L. Yuan, M.-Z. Yin, Internalization of hydroxyapatite nanoparticles in liver cancer cells, J. Mater. Sci. Mater. Med. 19 (2008) 1091–1095. doi:10.1007/s10856-007-3124-4.
[53] Y. Han, S. Li, X. Cao, L. Yuan, Y. Wang, Y. Yin, T. Qiu, H. Dai, X. Wang, Different Inhibitory Effect and Mechanism of Hydroxyapatite Nanoparticles on Normal Cells and Cancer Cells In Vitro and In Vivo, Sci. Rep. 4 (2014) 7134. doi:10.1038/srep07134.
[54] J. Solon, I. Levental, K. Sengupta, P.C. Georges, P.A. Janmey, F.C. MacKintosh, D. Stamenovic, F. Gallet, A. Bershadsky, L. Addadi, B. Geiger, V.M. Weaver, Fibroblast adaptation and stiffness matching to soft elastic substrates., Biophys. J. 93 (2007) 4453–61. doi:10.1529/biophysj.106.101386.
[55] C. Branco, D.D. Klumpers, W.A. Li, S.T. Koshy, J.C. Weaver, O. Chaudhuri, P.L. Granja, D.J. Mooney, Influence of the stiffness of three-dimensional alginate/collagen-I interpenetrating networks on fibroblast biology, Biomaterials. 35 (2014) 8927–8936. doi:10.1016/j.biomaterials.2014.06.047.

Figure captions

Figure 1. (a–c) SEM images of the HAp nanoparticles prepared by wet chemical precipitation methods at different temperatures (°C): (a) 30, (b) 50, and (c) 80. (d) Force-displacement curves for the PDMA gels glued by spreading 10 μL of pure water (gray line) and 10 μL of the 6 wt% S-HAp dispersion (black line). (e) Variations in the shear adhesion strength of the PDMA gels glued with the HAp dispersions. Error bars indicate standard deviations (N = 4). *At the same dispersion concentration, the adhesion strength for L-HAp was significantly different from those of S-HAp or M-HAp. The adhesion strengths of S-HAp and M-HAp showed no significant difference ($p<0.05$).

Figure 2. (a–c) SEM images of the nanoparticle-assembled plates prepared with (a) S-HAp, (b) M-HAp, and (c) L-HAp. The insets show the digital photographs of the plates. (d) Shear adhesion strengths of the PDMA gels glued with the HAp plates. Error bars indicate the standard deviations (N = 4). The numbers in the parentheses below the sample codes denote the number of samples that broke out of the adhesion area (the number of cohesive fractures of the adherends; see Fig. S4b)/total number of the samples. Different letters on the bars indicate the statistically significant difference ($p<0.05$).

Figure 3. (a) Sequential optical micrographs near the interface between a PDMA gel and an S-HAp plate. The images were binarized using ImageJ software (NIH). The S-HAp plate was relatively transparent in a dry state and turned opaque after the diffusion of water inside its pores. (b) Water diffusion distances inside the HAp plate after the gluing of PDMA and HAp. Error bars indicate the standard deviations (N = 3).

Figure 4. (a) The S-HAp plates could glue several kinds of mice soft tissues. (b) Mice skin tissues glued with an S-HAp plate (5 mm x 5 mm). A total weight of 30 g was applied on the bottom tissues. (c) Typical force-displacement curves and (d) shear adhesion strengths of the skin tissues glued with water (black), fibrin glue (blue), and the S-HAp plate (red). Error bars indicate the standard deviations (N = 4). Different letters on the bars indicate the statistically significant difference ($p<0.05$).

Figure 5. (i, ii) Optical micrographs of the histological sections of the skin tissues after H&E staining,

and SEM images of the surfaces of the (iii, iv) skin tissues and (v, vi) S-HAp plates (a) before and (b) after gluing. Each open square on the low magnification image represents the location corresponding to the high magnification image.

Figure 6. ATR FT-IR spectra of the (a) skin tissue and S-HAp plate (b) before and (c) after the adhesion with the skin tissues.

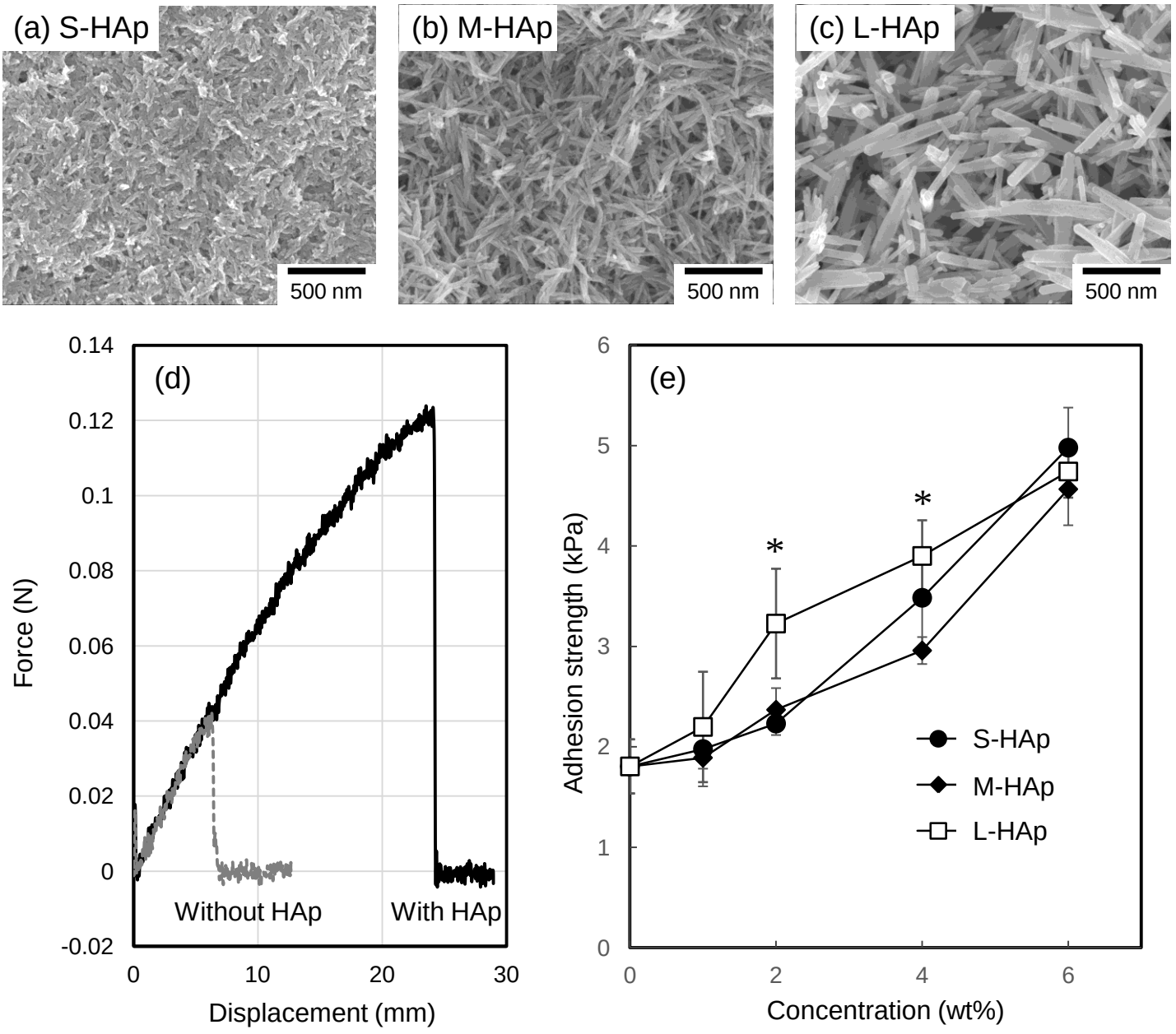

Figure 1. (a–c) SEM images of the HAp nanoparticles prepared by wet chemical precipitation methods at different temperatures (˚ C): (a) 30, (b) 50, and (c) 80. (d) Force-displacement curves for the PDMA gels glued by spreading 10 µL of pure water (gray line) and 10 µL of the 6 wt% S-HAp dispersion (black line). (e) Variations in the shear adhesion strength of the PDMA gels glued with the HAp dispersions. Error bars indicate standard deviations (N = 4). *At the same dispersion concentration, the adhesion strength for L-HAp was significantly different from those of S-HAp or M-HAp. The adhesion strengths of S-HAp and M-HAp showed no significant difference ($p<0.05$).

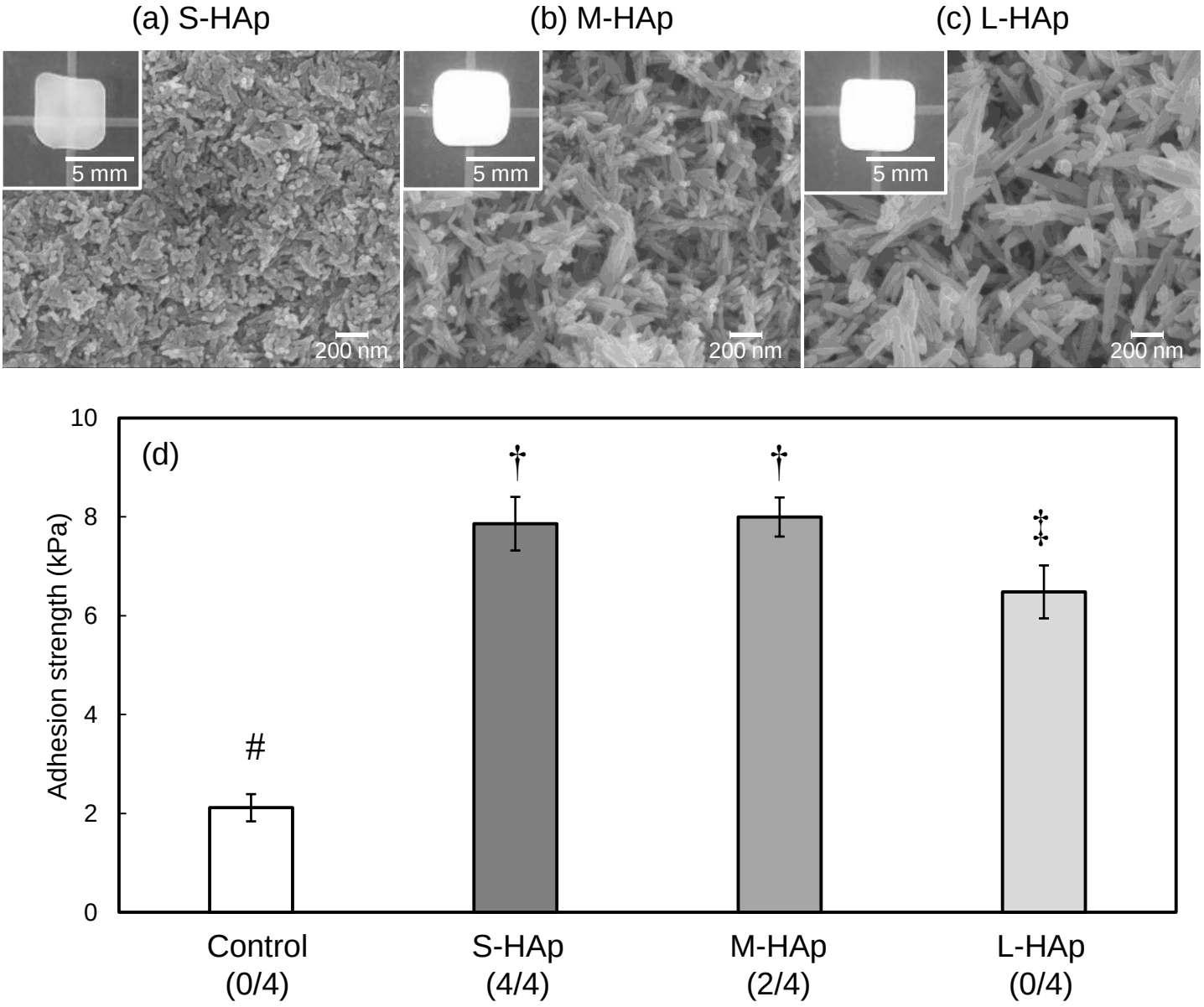

Figure 2. (a–c) SEM images of the nanoparticle-assembled plates prepared with (a) S-HAp, (b) M-HAp, and (c) L-HAp. The insets show the digital photographs of the plates. (d) Shear adhesion strengths of the PDMA gels glued with the HAp plates. Error bars indicate the standard deviations (N = 4). The numbers in the parentheses below the sample codes denote the number of samples that broke out of the adhesion area (the number of cohesive fractures of the adherends; see Fig. S4b)/total number of the samples. Different letters on the bars indicate the statistically significant difference ($p<0.05$).

(a) Optical microscope images near the interface between PDMA and HAp

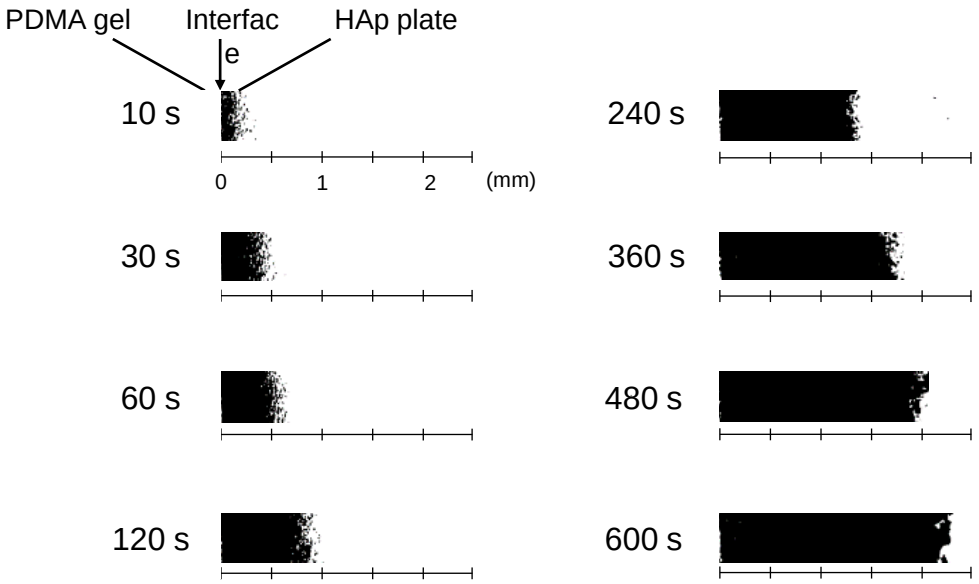

(b) Water diffusion distances inside HAp plate

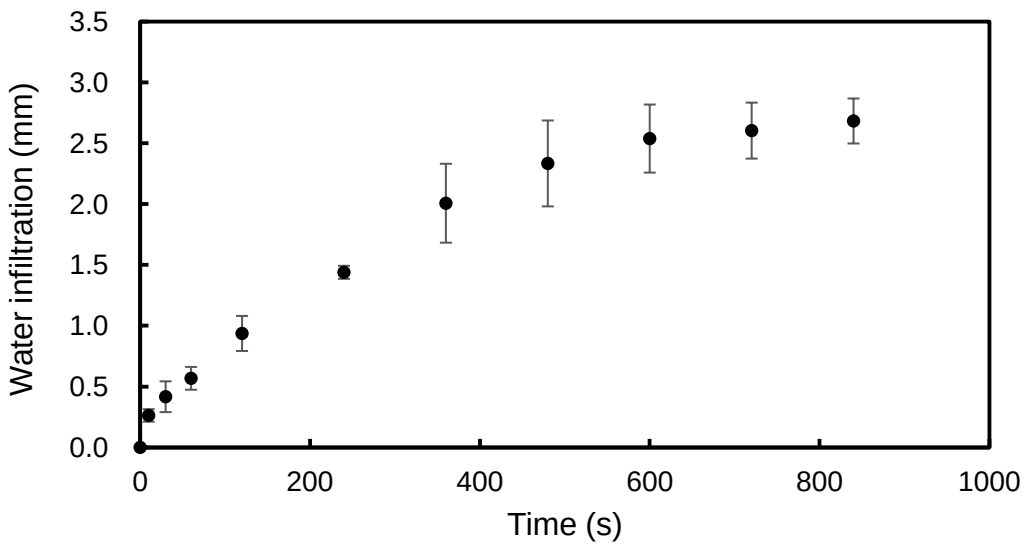

Figure 3. (a) Sequential optical micrographs near the interface between a PDMA gel and an S-HAp plate. The images were binarized using ImageJ software (NIH). The S-HAp plate was relatively transparent in a dry state and turned opaque after the diffusion of water inside its pores. (b) Water diffusion distances inside the HAp plate after the gluing of PDMA and HAp. Error bars indicate the standard deviations (N = 3).

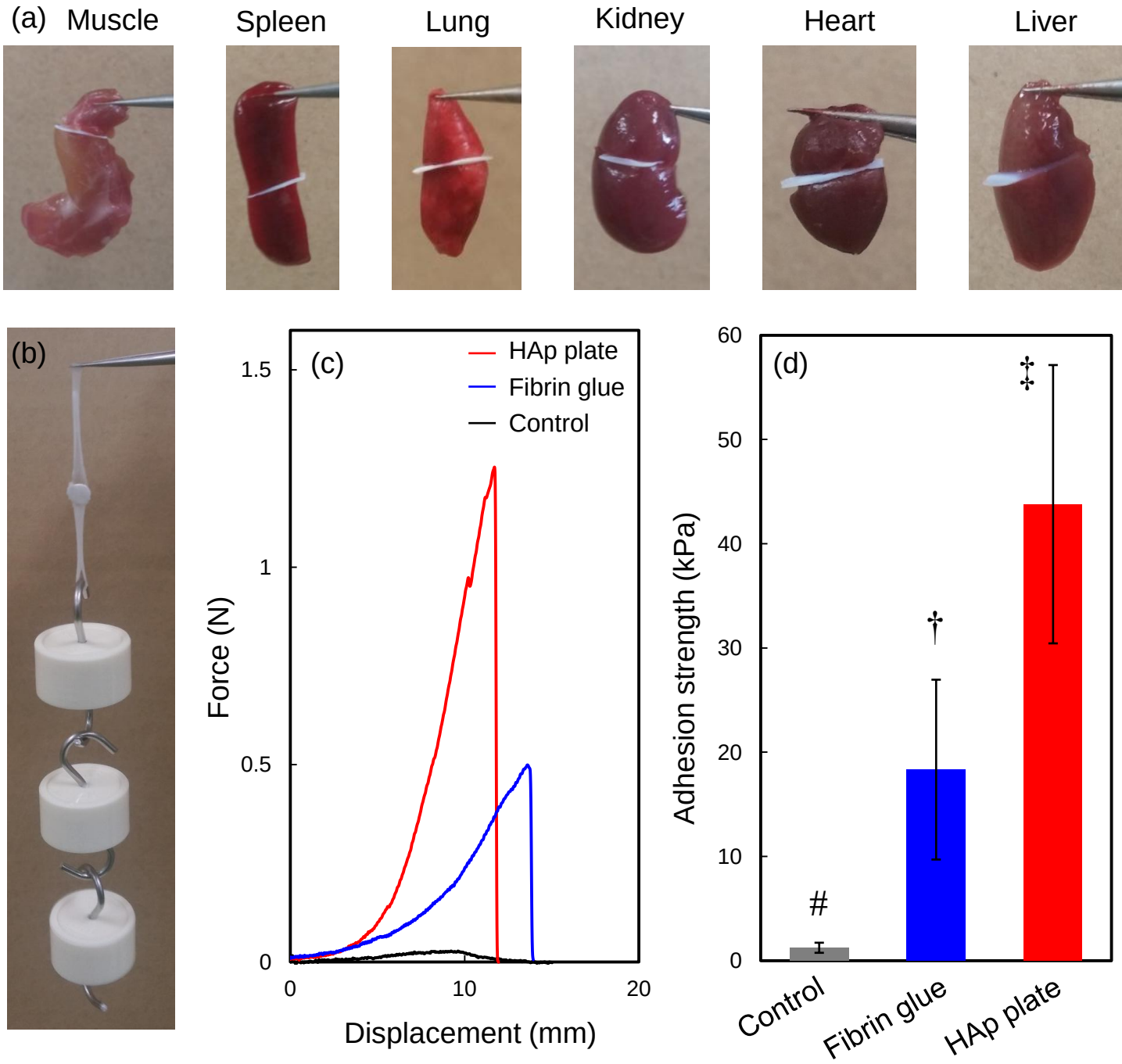

Figure 4. (a) The S-HAp plates could glue several kinds of mice soft tissues. (b) Mice skin tissues glued with an S-HAp plate (5 mm x 5 mm). A total weight of 30 g was applied on the bottom tissues. (c) Typical force-displacement curves and (d) shear adhesion strengths of the skin tissues glued with water (black), fibrin glue (blue), and the S-HAp plate (red). Error bars indicate the standard deviations (N = 4). Different letters on the bars indicate the statistically significant difference ($p<0.05$).

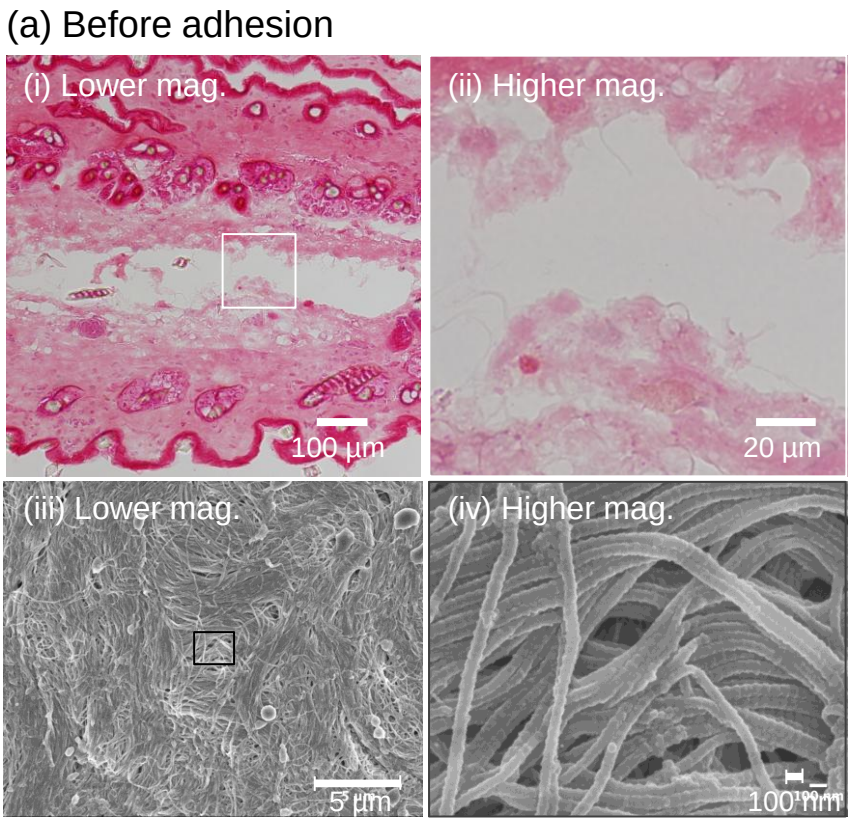

Figure 5. (i, ii) Optical micrographs of the histological sections of the skin tissues after H&E staining, and SEM images of the surfaces of the (iii, iv) skin tissues and (v, vi) S-HAp plates (a) before and (b) after gluing. Each open square on the low magnification image represents the location corresponding to the high magnification image.

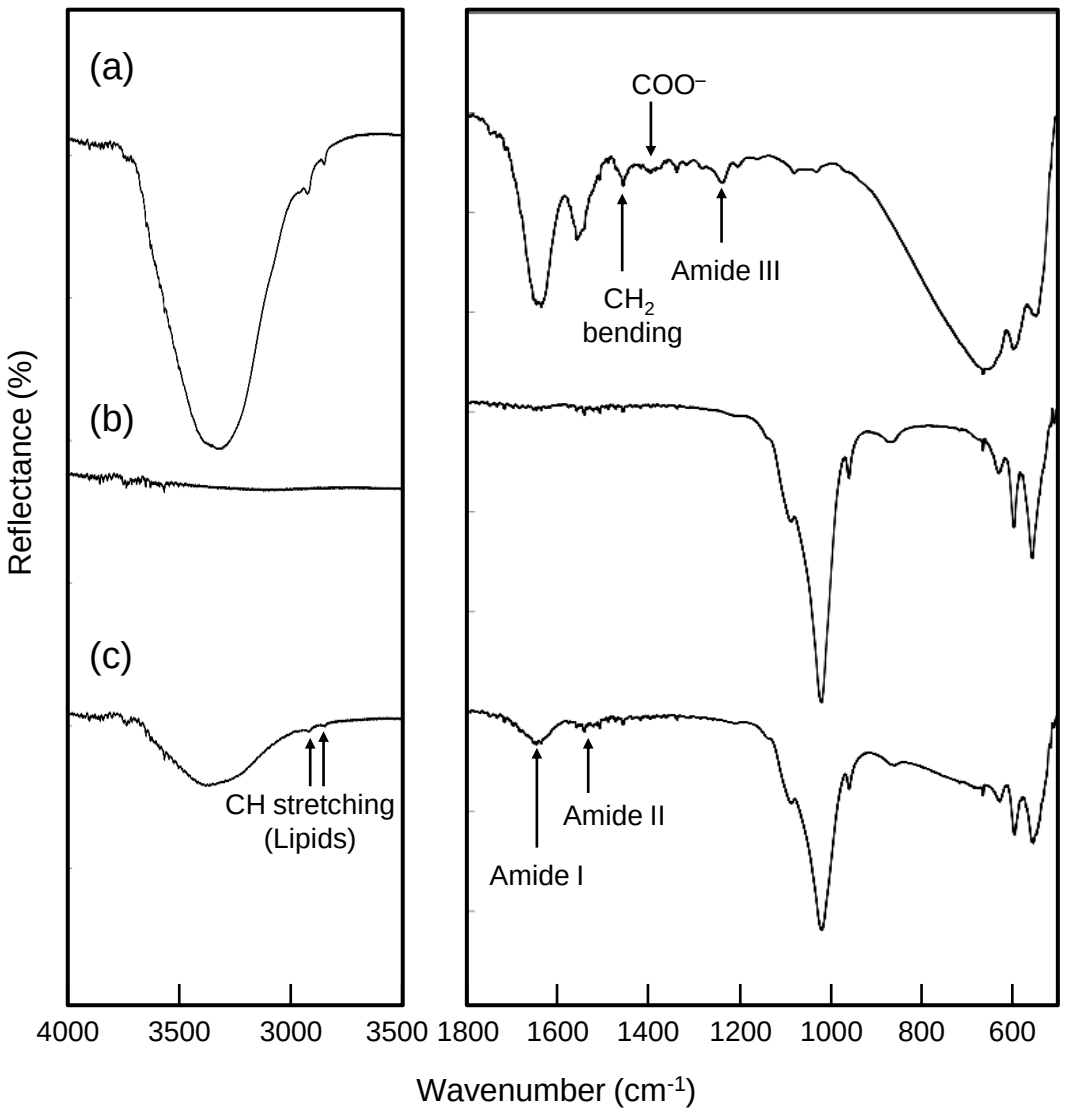

Figure 6. ATR FT-IR spectra of the (a) skin tissue and S-HAp plate (b) before and (c) after the adhesion with the skin tissues.

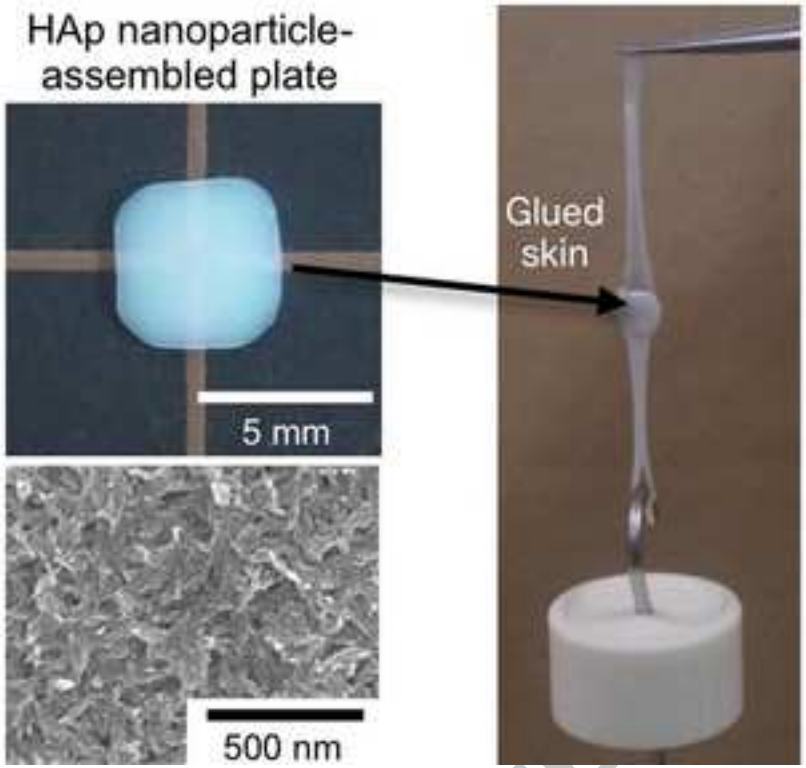

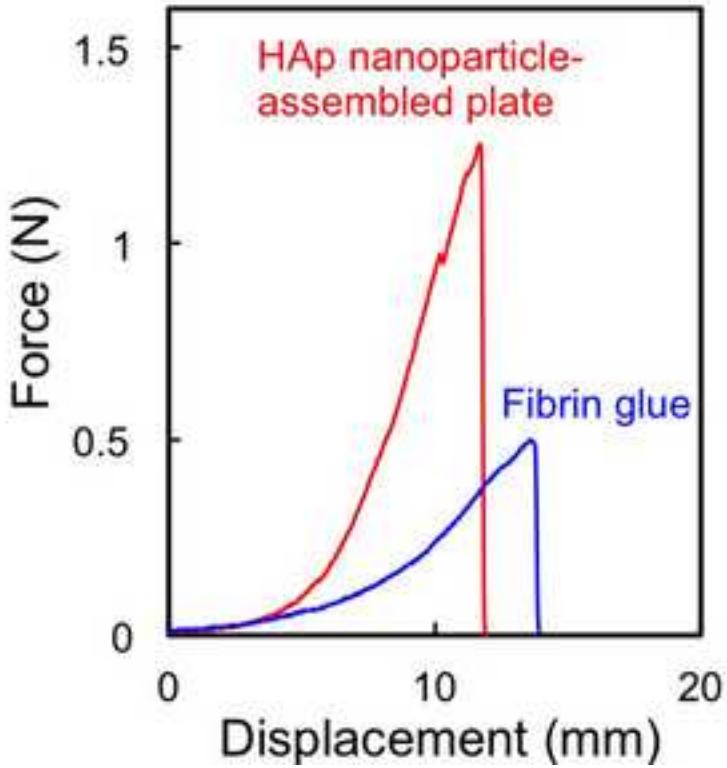

The present study indicates a new application of inorganic biomaterials (bioceramics) as a soft tissue adhesive.

Organic adhesives such as fibrin glues or cyanoacrylate derivatives have been commonly used clinically. However, their limited biocompatibility or low adhesion strength are some drawbacks that impair their clinical application. In this study, we synthesized a novel solid adhesive with biocompatible and biodegradable hydroxyapatite (HAp) nanoparticles without the aid of organic molecules, and showed an immediate and superior (i.e., 2.2 times higher) adhesion strength of mouse soft tissues compared to conventional fibrin glues. Given the importance of wet adhesion to biomedicine and biotechnology, our results suggest ways to develop new soft tissue adhesives as well as new applications of inorganic biomaterials.